Published in final edited form as:
Biomaterials. 2011 October ; 32(29): 7209–7216. doi:10.1016/j.biomaterials.2011.06.026.

Receptor-targeted Iron Oxide Nanoparticles for Molecular MR Imaging of Inflamed Atherosclerotic Plaques

Chuqiao Tu[a], **Thomas S.C. Ng**[b], **Hargun Sohi**[b], **Heather Palko**[c], **Adrian House**[a], **Russell E. Jacobs**[b], and **Angelique Y. Louie**[a,*]

[a]Department of Biomedical Engineering, University of California, Davis, CA 95616, USA.

[b]Beckman Institute, California Institute of Technology, Pasadena, CA 91125, USA.

[c]Department of Chemistry, University of California, Davis, CA 95616, USA.

Abstract

In a number of literature reports iron oxide nanoparticles have been investigated for use in imaging atherosclerotic plaques and found to accumulate in plaques via uptake by macrophages, which are critical in the process of atheroma initiation, propagation, and rupture. However, the uptake of these agents is nonspecific, thus the labeling efficiency for plaques *in vivo* is not ideal. We have developed targeted agents to improve the efficiency for labeling macrophage-laden plaques. These probes are based on iron oxide nanoparticles coated with dextran sulfate, a ligand of macrophage scavenger receptor type A (SR-A). We have sulfated dextran-coated iron oxide nanoparticles (DIO) with sulfur trioxide, thereby targeting our nanoparticle imaging agents to SR-A. The sulfated DIO (SDIO) remained mono-dispersed and had an average hydrodynamic diameter of 62 nm, an r_1 relaxivity of 18.1 $mM^{-1}s^{-1}$, and an r_2 relaxivity of 95.8 $mM^{-1}s^{-1}$ (37 °C, 1.4 T). Cell studies confirmed that these nanoparticles were nontoxic and specifically targeted to macrophages. *In vivo* MRI after intravenous injection of the contrast agent into an atherosclerotic mouse injury model showed substantial signal loss on the injured carotid at 4 and 24 hours post-injection of SDIO. No discernable signal decrease was seen at the control carotid and only mild signal loss was observed for the injured carotid post-injection of non-sulfated DIO, indicating preferential uptake of the SDIO particles at the site of atherosclerotic plaque. These results indicate that SDIO can facilitate MRI detection and diagnosis of vulnerable plaques in atherosclerosis.

Keywords

Nanoparticles; Imaging agents; MRI (magnetic resonance imaging); Molecular imaging; Macrophages; Inflammation

*Corresponding author. Department of Biomedical Engineering, University of California, Davis, CA 95616, USA. Tel.: 1 530 7527134; fax: 1 530 7527156. aylouie@ucdavis.edu (A. Y. Louie).

Supporting Information Available

Cytotoxicity of dextran sulfate and the influence of incubation time on particle uptake by cells, six videos for MR imaging of neck/carotid region pre-injection and 4h, 24h post-injection of SDIO or DIO contrast agents, etc.

1. Introduction

Cardiovascular disease (CVD) is the leading cause of death in the western world and its prevalence is expected to increase further during the next 3 decades.[1] Increasing evidence indicates that it is atherosclerotic plaque rupture rather than severity of vessel occlusion that leads to major adverse events, such as stroke and myocardial infarction.[2–3] Early detection of unstable plaques would be of great value to guide treatment decisions, with the aim to decrease morbidity/mortality in affected patients. There is an intense focus in the field to identify specific biomarkers that indicate a plaque's risk for rupture and develop noninvasive methods to detect those markers.[1, 4–5] Magnetic resonance imaging (MRI) has played a prominent role in anatomical and functional examinations of the major vessels; however, without signal enhancement, the technique lacks sufficient sensitivity to directly detect and identify biomarkers of interest.[6–7]

Recent advances in the development of MRI contrast agents (CAs), which specifically target relevant biomarkers and enhance images to generate sufficient contrast in tissues and organs of interest, allow MRI to visualize molecules and molecular events occurring at a cellular level.[6, 8] However, the amount of biomarkers in the cardiovascular system is usually expressed in the low nanomolar range ($\leq 10^{-9}$ mol/g of tissue), which is below the detection sensitivity of routinely used gadolinium chelates (10^{-7} mol/g of tissue). Particle-based technologies provide an effective method to concentrate signal-generating materials into a relatively small entity, which can greatly improve their detectability ($10^{-10} – 10^{-11}$ mol/g of tissue) *in vivo*.[7, 9–10] Moreover, the particle CAs have a large surface areas, allowing them to display more targeting ligands, further enriching the CAs at the region of interest (ROI).

Non-toxic and biocompatible iron oxide nanoparticles (IO NPs) have been widely used as MRI CAs in the clinic.[11] IO NPs, however, are generally non-specific; they show a differential distribution in the body based primarily on relative tissue permeability. We are interested in the development of IO NP CAs that target biomarkers of atherosclerotic plaques. In the search for markers to identify high-risk plaque, macrophages have been found to correlate with plaque stability --- plaques with high macrophage content tend to be more unstable, and the distribution pattern for the macrophages can be indicative of degree of stability.[12–13] IO NPs have been used for MRI detection of plaques in pre-clinical experiments using different animal models of atherosclerosis, and the results showed that these particles accumulate in plaque macrophages.[14] However, the uptake of IO NPs by macrophages is nonspecific through phagocytosis. This is an inefficient process that provides relatively weak contrast between the plaque and surrounding tissues.[15]

We have previously developed CAs based on the scavenger receptor type A (SR-A) targeting ligands maleylated BSA and dextran sulfate.[16–18] SR-A is highly expressed on activated macrophages and not found on normal vessel walls.[19] These probes labeled atherosclerotic plaques with improved efficiency over non-targeted probes. However, it was difficult to obtain mono-dispersed IO NPs by synthesizing them using either dextran sulfate, or a combination of dextran sulfate and dextran, as a starting materials to form the coating.[20] In this work, we introduce a new synthetic method in which we coated IO NPs with dextran (DIO), then sulfated the dextran coating of the particles to make dextran sulfate coated IO NPs (SDIO). The ability of SDIO to target macrophages *in vitro* and to detect and access macrophages in atherosclerotic plaque *in vivo* was evaluated by MRI.

2. Materials and methods

2.1. Materials

Materials were obtained from commercial suppliers and used directly, unless otherwise noted. Dextran (from leuconostoc, average mol. wt. 9,000–11,000) and ferric chloride hexahydrate ($FeCl_3 \cdot 6H_2O$, Fw 270.29 g/mol) were purchased from Sigma-Aldrich. Ferrous chloride tetrahydrate ($FeCl_2 \cdot 4H_2O$, Fw 198.81 g/mol) and dextran sulfate (sodium salt, prepared from dextran from leuconostoc SSP., average mol. wt. 5,000) were acquired from Fluka. Ammonium hydroxide (28–30%), sodium bicarbonate and sodium hydroxide were provided by Fisher Scientific. Sulfur trioxide pyridine complex, sulfur trioxide DMF complex and 2-methyl-2-butene (2M2B) were purchased from Acros. Anhydrous formamide was purchased from MP, Biomedicals, LLC. Spectra/por® dialysis membrane (mol. wt. cut-off 50,000) was purchased from Spectrum Laboratories, Inc. P388D1 cells and RPMI-1640 medium were obtained from American Type Culture Collection (ATCC). Fetal bovine serum (FBS), L-glutamine, PBS (1X) and C_{12} – Resazurin were provided by GIBCO. Lipoprotein deficient bovine serum (LPDS) was obtained from Biomedical Technologies, Inc. (Stoughton, MA). Water was purified using a Millipore Milli-Q Synthesis purifier (18.0 MΩ cm, Barnstead).

2.2. Synthesis of dextran sulfate coated iron oxide nanoparticles

Dextran coated iron oxide nanoparticles (DIO) were synthesized as previously reported.[20] The DIO (200 mg) was dissolved in 10 mL of dry formamide. After complete dissolution, 2-methyl-2-butene (2M2B) (1.6 mL, 15 mmol) was slowly added to the flask under argon atmosphere and magnetic stirring. A SO_3–pyridine complex (0.32 g, 2 mmol) was rapidly added, and the reaction mixture was stirred at 30 °C under argon atmosphere for 2 h. The reaction was quenched by slowly pouring it into 7 mL of saturated sodium bicarbonate solution. After the final product was concentrated, the residue was dissolved in water and was dialyzed against deionized water in a dialysis bag with molecular weight (MW) cut-off of 50,000 Dalton for 72 h (8–10 changes of water). The solution was lyophilized to give a brown solid.

2.3. Characterization of SDIO

The iron oxide core size of SDIO and DIO were measured by transmission electron microscopy (TEM) on a Philips CM-12, operating at 80 kV. The average hydrodynamic particle size and size distribution of SDIO and DIO were measured using dynamic light scattering (DLS) with a Nanotrac 150 particle size analyzer (Microtrac, Inc., Montgomeryville, PA). The zeta potential (ζ) values of SDIO and DIO were measured by determining the electrophoretic mobility using a NICOMP™ 380 ZLS device (Particle Sizing Systems, Inc., Santa Barbara, CA, USA) in deionized water at room temperature. Elemental analysis was performed by Columbia Analytical Services of Tucson, Arizona. FT-IR spectra were collected on a Shimadzu IR Prestige 21 spectrophotometer.

Longitudinal (T_1) and transverse (T_2) relaxation times were measured at 60 MHz (1.4 T) and 37 °C on a Bruker Minispec mq60 (Bruker, Billerica, MA). Three stock solutions of SDIO were prepared by dissolving appropriate amounts of particles in pH 7.0 deionized water. The concentration of iron was determined by ICP-MS. The stock solutions were diluted to give three series of aqueous solutions with decreasing iron concentration (0.3 mL each). All solutions were prepared by weight. Iron concentrations were calculated based on the concentration of the stock solution and appropriate dilution factors. T_1 values were measured using an inversion recovery sequence with 10–15 data points and T_2 values were measured using a Carr–Purcell–Meiboom–Gill (CPMG) sequence with $\tau = 1$ ms, and 200 data points. Each solution was incubated at 37 °C for 10 min before measurement. The longitudinal (r_1)

and transverse (r_2) relaxivity were determined as the slope of the line for plots of $1/T_1$ or $1/T_2$, respectively, against increasing iron concentration with a correlation coefficient greater than 0.99.[21] The relaxivity of DIO was measured by the same procedure. The T_1 and T_2 relaxation times of cell lysates containing SDIO or DIO were also measured with the method described above.

2.4. Cell experiments

2.4.1. Cell culture—The P388D1 cells were maintained in tissue culture flasks (75 cm^2) in media (RPMI-1640 with 1% L-glutamine and 10% fetal bovine serum (FBS)) at 37 °C in a humidified environment of 5% CO_2 atmosphere. When the cells reached 80–90% confluence, the medium was removed. The cells were scraped down with a rubber policeman and used for either sub-culture or *in vitro* cell studies. All experiments were performed on cells that were passaged an equal number of times.

2.4.2. In vitro cellular uptake of SDIO and DIO—The P388D1 cells were plated to 60 mm diameter tissue culture dishes at 1×10^6 cells/mL of RPMI-1640 with 1% L-glutamine and 10% lipoprotein deficient bovine serum (LPDS) (2 mL per dish). The cells were maintained in media at 37 °C in a humidified environment of 5% CO_2 atmosphere overnight which allowed cells to adhere to the bottom of dishes.

Three stock solutions of SDIO or DIO were prepared by dissolving appropriate amount of particles in RPMI-1640 with 1% L-glutamine and 10% LPDS. The concentration of iron was determined by ICP-MS. The stock solutions were diluted with media to give series of three solutions with decreasing iron concentration. All solutions were prepared by weight and iron concentrations were calculated based on the concentration of the stock solution and appropriate dilution factors. The resultant media solutions of SDIO or DIO were incubated in 37°C water bath for 20 min before use. After removal of maintenance media, the SDIO or DIO medium solutions were introduced to the cells and incubated at 37 °C in 5% CO_2 atmosphere for 2 h. After removal of the media, cells were washed with 1X PBS (37 °C) (3 × 2 mL for each dish, ~ 2 min for each washing). Deionized water was added in dishes (1.2 mL for each dish), and the freeze-thaw (30/20 min) method was repeated twice to lyse cells. The cell lysates were put into 1.5 mL conical tubes and lyophilized. Deionized water was added to the residue (0.3 mL each) to generate solutions for relaxation time measurement.

2.4.3. Specificity of Uptake—To verify that cellular uptake was receptor-specific, competition experiments were conducted and characterized by relaxation times. The P388D1 cells were incubated with SDIO ([Fe] = 5.0×10^{-5} M) in the presence of competing dextran sulfate or non-competing dextran as control in 0, 0.02, 0.1, 0.4, 1, and 10-fold excess concentrations. Cells were incubated at 37 °C in a 5% CO_2 atmosphere for 2 h and then prepared for relaxation time measurement as described previously.

2.4.4. Cytotoxicity—Cytotoxicity of SDIO was evaluated with P388D1 cells using the C_{12} - Resazurin viability assays. P388D1 cells in RPMI-1640 were plated in 96-well dishes at a concentration of 1.1×10^4 cells per well. This places the cells at a density for linear growth rate which is optimal for the assay. After overnight incubation in 5% CO_2 atmosphere at 37°C, the existing RPMI-1640 was replaced with fresh media containing varying amounts of SDIO. Cells were incubated with SDIO for either 4 or 24 h. The media were removed and cells were washed with 1X PBS three times, then media containing C_{12} - Resazurin (5 μM) was added. After incubation for 15 minutes for reduction of the compound, fluorescence was measured using a Safire^2 monochromator microplate reader (Tecan Austria G.M.B.H., Austria) with excitation of 563 nm and an emission of 587 nm. Samples were performed in triplicate to provide statistical significance.

2.5. Animal studies

2.5.1. Animal model—All animal experiments were performed under protocols approved by the Animal Care and Use Committee of the University of California, Davis and the California Institute of Technology. Apo $E^{-/-}$ mice (12 weeks old, Jax West Laboratories, West Sacramento, CA) were used for the experiments. Either the right or left carotid artery of each mouse was ligated two weeks before imaging. Subsequent to ligation, mice were placed on a high fat diet (TD.88137, Harlan Laboratories Inc., Madison, WI). To perform the ligation a medial incision was made between the mandible and clavicle, exposing the glands and vessels of the neck. The carotid artery was singled out from the surrounding tissue, with much attention given to protecting and excluding the parallel-running vagus nerve. A 6/0 silk suture was threaded under the dorsal side of the carotid artery and was tied off to cause injury to the site. The procedure was concluded with five to six discontinuous 4/0 ethilon sutures to reconnect the skin of the original ventral incision. The mice were monitored twice a day for approximately four days to check for irritation and to administer analgesics when appropriate.

2.5.2. In vivo MRI—All images were acquired on a 7T (Bruker Biospec) small animal magnet using a home-built birdcage coil. For all time points, the animal was anesthetized with an 1.5% isofluorane:air mixture, kept at 35–37°C with warm air flowing through the bore and the respiration was monitored (MP150, Biopac, Goleta, CA). After localizing the ROI around the neck using a RARE spin echo sequence (TR/TE = 4000/22ms, matrix size = 128×128, FOV = 35.35×35.35mm^2, slice thickness = 0.754mm), the common carotid arteries were located with a time-of-flight angiography sequence with venous saturation (FL2D_ANGIO method, Paravision 4.0: TR/TE = 13.7/3.5ms, matrix size = 150×100; zero-filled to 256×100, FOV = 30×20mm^2, slice thickness = 0.754mm). A gradient echo sequence was then utilized to visualize the uptake of SDIO/DIO particles (TR/TE=1000/5ms, F.A. = 35°, matrix size = 200×200; zero-filled to 256×200, FOV = 35.35×35.35mm^2, slice thickness = 0.754mm) at the region of the common carotid arteries. A set of pre-injection images was acquired one day prior to injection. For particle injection, 30 mg/kg Fe content of SDIO (n = 3) or DIO (n = 2) particles dissolved in saline were injected via the tail vein. The imaging protocol was then repeated at 4 hours and 24 hours post injection.

2.5.3. MR images analysis—To analyze the acquired images, all gradient echo images were first reconstructed such that the intensity scaling and offset of all images for each mouse were equivalent. To compare particle uptake between timepoints and subjects, we define a contrast ratio (CR) metric as:

$$\mathrm{CR}=\frac{\left|\frac{[I_{\mathrm{ligated}}]-[I_{\mathrm{brain}}]}{[I_{\mathrm{control}}]-[I_{\mathrm{brain}}]}\right|_{i}}{\left|\frac{[I_{\mathrm{ligated}}]-[I_{\mathrm{brain}}]}{[I_{\mathrm{control}}]-[I_{\mathrm{brain}}]}\right|_{\mathrm{prescan}}}$$

Where I_{ligated} is the mean intensity of the region of interest (ROI) drawn around the ligated carotid artery, I_{control} is the mean intensity of the ROI drawn around the contra-lateral carotid. I_{brain} is the mean intensity of the ROI drawn in the spinal cord at the same image slice as the other ROIs and *i* is either 4 or 24 hours post-injection timepoints. ROIs were drawn manually at slice levels approximately located at the common carotid arteries. These were matched between timepoints. Angiography images were used to guide ROI delineation around the carotid arteries. Because previous reports noted that the carotid vessels along with the wall are ~1 mm in diameter,[22] all arterial ROIs had diameters of 1.5 mm. CR for

SDIO injected mice and DIO injected mice were compared using a two-sided t-test in Microsoft Excel.

3. Results and Discussion

3.1. Synthesis of SDIO

The DIO were synthesized according to our previously reported procedure.[20] The sulfation of polysaccharides has been reported via both heterogeneous and homogeneous synthesis pathways. Heterogeneous sulfation reactions with chlorosulfonic acid are subject to major drawbacks such as multiple and non-reproducible side reactions, presence of hazardous and non-reproducible sulfation rates and patterns, and backbone degradation. Homogeneous sulfation of dextran with nitrogen base complexes of sulfur trioxide in aprotic solvents are the preferred method; however, homogeneous reactions are still accompanied by some non-reproducible side reactions such as cleavage of labile functional groups and backbone degradation.[23] Our first effort to sulfate DIO followed literature methods, which performed sulfation of dextran with sulfur trioxide pyridine complex in dry formamide at room temperature.[24] However, the resultant particles showed 2 size peaks with an average hydrodynamic diameter of 122 ± 97 nm. The sulfation reaction was reassessed under different synthetic conditions including varying temperatures, using sulfur trioxide DMF complex as sulfating agent, or using DMF as reaction solvent, yielding similar results. This indicates that although sulfation of dextran with nitrogen base complexes of sulfur trioxide is well-known,[23] successful translation to a dextran coat on a nanoparticle is not trivial. The larger-sized peak may have been due to the depolymerization of dextran followed by aggregation of incompletely coated iron oxide nanoparticles.

Sulfur trioxide pyridine complex is made by dripping chlorine sulfate acid into dry pyridine at −15 °C.[24] However, the presence of pyridine may only partially limit the highly acidic character of chlorosulfonic acid, which is known to be responsible for multiple, undesirable, and non-reproducible side reactions such as cleavage of acid labile functional groups and partial depolymerization.[25] We therefore introduced an acid scavenger of a neutral nature, 2-methyl-2-butene (2M2B), into the reaction before the addition of sulfation agent, hypothesizing that this would clear the free acid produced in the system in a timely fashion and lead to a more efficient reaction, with diminished side reactions in the sulfation of dextran coat on IO NPs (Scheme 1).[25–26] The purified, sulfated DIO were turned out to be mono-dispersed nanoparticles.

3.2. Characterization of SDIO

3.2.1. SDIO formation verification—Successful sulfation was verified by infrared spectroscopy and elemental analysis of the purified particles. Compared to the infrared spectrum of DIO, new absorptions of S=O groups at 1234 cm^{-1} (asymmetrical stretch), 1011 cm^{-1} (symmetrical stretch), and 826 cm^{-1} (symmetrical C-O-S stretch) were observed, while the absorptions at 3426 cm^{-1} (O-H stretch) and 1026 cm^{-1} (C-O stretch) were decreased in the infrared spectrum of SDIO.[24] The emergence of sulfur (9.74%) and decrease of iron content (from 17.7% in DIO to 11.34% in SDIO) in SDIO further verified successful sulfation of DIO. The results from elemental analysis of sulfur content also showed that a two-hour reaction time was sufficient for the sulfation of DIO; longer reaction time did not appear to increase sulfation.

3.2.2. SDIO size, relaxivity and surface charge—SDIO has an average core size of 7–8 nm (Figure 1a) and an average hydrodynamic diameter of 62.4 nm (Figure 1b), an r_1 relaxivity of 18.1 $mM^{-1}s^{-1}$, and an r_2 relaxivity of 95.8 $mM^{-1}s^{-1}$ (37 °C, 1.4 T) in pH 7.0

deionized water. The r_2 to r_1 ratio was 5.4, indicating that SDIO could be used, preferably, as a T_2-weighted MRI contrast agent.

The measured zeta potential (ζ) values were − 14.90 mV and − 40.05 mV for DIO and SDIO, respectively. Typically the ζ value reflects the electric charge on the particle surface and indicates the physical stability of dispersions and emulsions in a colloidal system.[27] Double layers with high ζ values would create powerful electrostatic repulsion and, consequently, prevent aggregation resulting from collisions caused by Brownian motion. In comparison with DIO, the ζ value of SDIO decreased by 25.15 mV, indicating a more stable dispersion and emulsification of SDIO in water. In practice, we found SDIO to be very stable, with a long shelf life in aqueous solution. We have not observed any properties to change (e.g. aggregation, size, and magnetic property) after benchtop storage for over a year at room temperature.

Dextran in DIO is coated on the surface of iron oxide core. Due to decreased access for hydroxyl groups that lay deeper in the polymer layer, we estimate that the degree of sulfation of outer polymer layer is greater than that of the inner polymer layer. This should be ideal because the maximum sulfation of surface dextran can greatly increase the targeting ability of the nanoparticles to macrophages with less charge repulsion at the inner polymer layers that can affect size and MRI properties. Particle size was somewhat larger in comparison with that of non-sulfated DIO. This is likely due to the repulsion of negatively charged sulfate groups on the surface of SDIO. The r_1 and r_2 relaxivity values of SDIO were similar to those of DIO. This is not unexpected as the size of the iron oxide cores was similar for DIO and SDIO. Reproducibility of our method was validated by repeating the same reaction; running the reaction with a different scale of DIO; and using sulfur trioxide DMF complex as sulfation agent instead of sulfur trioxide pyridine complex. All of these reactions gave similar products, indicating that our sulfation procedure is reproducible and robust.

3.3. Cell experiments

3.3.1. SDIO targeting to macrophages P388D1—We selected SR-A as the target for our particles because it is highly expressed on activated macrophages in atheromas. SR-A recognizes and binds a number of polyanionic molecules, such as oxidized LDL, that contribute to the involvement of macrophages in the formation of plaques.[28] For example, experiments conducted on Apo E knockout (Apo $E^{-/-}$) mice demonstrated that knocking out SR-A resulted in a significant decrease in atherosclerotic plaque size.[29] To demonstrate targeting of SDIO to macrophages, we performed *in vitro* studies using P388D1 murine macrophage cells. Uptake of DIO was also performed as a control for comparison; the properties of the DIO particles were similar to those of the commercially available MRI CA Sinerem (Table 1).[30]

The T_2 values of the lysates of macrophages incubated with increasing concentrations of SDIO or DIO for 2 hours are shown in Figure 2. In comparison with DIO, the mean T_2 values were significantly lower for cell lysates incubated with SDIO at all concentrations. In comparison with the lysates of blank macrophages, SDIO at 5.0×10^{-5} M Fe significantly decreased T_2 by 70% (p value = 0.002), compared to a 20% T_2 decrease (p value = 0.03) for the same iron concentration of DIO, indicating that there was limited uptake of DIO compared to SDIO under the same conditions. This result was as expected because DIO is not a ligand of SR-A so it is not recognized by the receptor. Our results demonstrate that sulfation of DIO facilitates SR-A targeting, and greatly improves accumulation of the particles in macrophages over the non-targeted, dextran coated particles.

3.3.2. Receptor-mediated uptake of SDIO by macrophages P388D1—Specificity for the cellular uptake of SDIO was confirmed by competition studies in which cells were incubated with a fixed concentration of SDIO and increasing excess of unlabeled dextran sulfate (ligand of SR-A) or dextran (not a ligand of SR-A). If uptake of the agents was receptor-mediated, the excess unlabeled ligand should compete for binding to the receptors. Nonspecific uptake is strictly concentration-dependent and would not be affected by additional ligands in the solution.[16, 31] Receptor-mediated uptake of SDIO was confirmed by the results seen in Figure 3: increasing amounts of competitor, from 0.02 to 10-fold excess, strongly reduce uptake, while increasing amounts of excess dextran had little influence on the uptake, indicating that the uptake of SDIO by SR-A is a receptor-mediated process. To exclude the possibility that the reduced uptake of SDIO in the presence of dextran sulfate is caused by toxicity or any other influence of dextran sulfate on the cells themselves, dextran sulfate alone, at the same concentrations, was applied to P388D1 cells in culture and the cell viability was evaluated by the C_{12} - Resazurin viability assay.[32] The average cell viability was above 96% after either 4 h or 24 h incubation of cells with the concentration of dextran sulfate varying from 0.04 to 10×10^{-3} M, indicating that the dextran sulfate is not toxic to mammalian cells (Supplementary Figure 1).

3.3.3. Cytotoxicity of SDIO to mammalian cells—As a preliminary assessment of SDIO's toxicity to cells, SDIO were applied to P388D1 cells in culture and the cell viability was evaluated by the C_{12} - Resazurin viability assay.[32] Untreated cells served as negative control. The average cell viability is above 96% or 94% after 4 h or 24 h incubation with the particles varying from 0.02 to 5×10^{-3} M iron, respectively (Figure 4). The result showed that SDIO at concentrations relevant for biological imaging do not have observable toxicity to mammalian cells. This is similar to the results for most of the *in vitro* cytotoxicity studies on iron oxide nanoparticles reported in the literature.[33–36]

A major concern that limits the use of nanomaterials in clinic is the potential toxicity. The iron oxide nanoparticles have been used in the clinic due to their biocompatiblity. After injection the IO NPs are taken up in the liver and spleen where they are metabolized and broken down slowly to release free iron ions. The released iron ions are added to the body's iron stores and eventually incorporated by erythrocytes as hemoglobin.[37] Free iron ions could potentially be cytotoxic because of the catalytic function of iron in the production of reactive oxygen species (ROS), which in turn can cause lipid peroxidation, protein oxidation, and DNA damage. However, the body has the ability to process these released iron ions as indicated by iron's large median lethal dose (LD_{50}) of 450 mg/kg for oral ingestion in the rat model.[10, 14] In fact, iron oxide nanoparticle MRI contrast agents have maintained an excellent safety record since they were approved for clinical use.[37–38]

3.4. Animal studies

The Apo $E^{-/-}$ mouse is a widely accepted model for atherosclerosis. In practice, we found that ligation of carotid arteries was an effective method to generate macrophage laden plaques.[18] The carotid artery is relatively superficial and more amenable to surgical procedures than the coronary artery. Therefore, to evaluate the preliminary *in vivo* capabilities of SDIO we utilized a carotid ligation model. A single carotid artery in the Apo $E^{-/-}$ mouse (n= 5) was ligated two weeks prior to the imaging study to induce atherosclerotic plaques. A T_2^*-weighted MRI with gradient echo sequence was utilized to visualize the uptake of SDIO and DIO particles. Image slices from a representative mouse, matched at the same slice level of the mouse common carotid arteries over a 24-h time course are shown in Figure 5a.

Because SDIO is a negative contrast agent, regions taking up SDIO produce a T_2^* susceptibility effect, appearing darker than areas without SDIO. The MR images displayed a sizeable decrease in the signal of the ligated carotid artery at 4 and 24 h compared to the pre-injection image. The result parallels that from the *in vitro* particle incubation time study that showed that T_2 values of the lysates of macrophages incubated with SDIO decreased substantially after a 4h incubation time with little subsequent change (Supplementary Figure 2). No discernable signal decrease was seen on the control carotid artery. This suggests preferential uptake of the SDIO particles at the sites of atherosclerotic plaque. Image slices from a representative mouse injected with DIO particles is shown in Figure 5b. Compared to SDIO injected animals, less signal intensity decrease was seen over time for the DIO injected subjects. Visualization of the volume regions above and below each slice depicted in Figure 5, shown in Supplementary Videos 1–6, confirmed that the signal decreases observed were due to localization of contrast agent, and not in homogenities in endogenous signal between slices.

To compare the relative uptake between SDIO and DIO particles in a more quantitative manner, we define a contrast ratio (CR) metric to measure the magnitude of signal decrease at the arterial site. As seen in Figure 6, the CR of SDIO injected mice were significantly higher than those of the DIO injected mice by 4 h post injection (p value = 0.03). This suggests that at the same injected iron dose, SDIO accumulated preferentially compared to DIO particles at the site of atherosclerotic plaque. It should be noted that the ROIs delineated included the signal contribution of particles in the blood. We normalize for this effect by comparing between the left and right carotids, which factors out the signal contribution due to blood borne particles.

Iron oxide nanoparticle-enhanced MRI has been reported to be able to identify atherosclerotic plaques in both *in vivo* animal and human studies.[14] However, the non-specific contrast agents are taken up by activated macrophages in vulnerable plaques via phagocytosis, pinocytosis or fluid-phase transport, which are inefficient processes.[15] As a result, direct visualization of atherosclerotic plaques often required relatively large amounts of nanoparticles.[14, 39] A tissue-specific contrast agent would allow for an improved identification of these lesions.[38, 40] Active targeting of nanoparticles can be achieved by decorating them with a ligand against a known marker associated with lesions. Our *in vivo* MRI images revealed that at 4 h post-injection, targeted SDIO provided a 4-fold increase in the contrast ratio compared to non-targeted DIO. The contrast ratio metric was used to account for differences in anatomy and physiology between subjects. Comparing the signal decrease between the ligated and control artery region normalizes the metric and allows cross comparisons over timepoints and between subjects. It should be noted that the ROIs delineated included the signal contribution of particles in the blood. We normalize for this effect by comparing between the left and right carotids, which factors out the signal contribution due to blood borne particles. Comparison between the CR of SDIO versus DIO injected mice (Figure 6) suggests a time-dependence for optimal SDIO uptake. This is likely to be a function of the degree of vulnerability of the plaque at the local site as well as the general pharmacokinetics of the particles. Future studies will aim to correlate this with *ex-vivo* assays to further understand the mechanism of particle accumulation.

We have previously shown the SR-A is a viable target for labeling macrophages and atherosclerotic plaques.[16–17] Recently, micelles containing gadolinium chelates and antibodies against SR-A have been synthesized and applied to MRI of aortic plaques in Apo $E^{-/-}$ mice. *In vivo* MRI revealed that at 24 h postinjection, targeted micelles provided a 79% increase in signal intensity of atherosclerotic aortas compared with 34% using non-targeted micelles, and no enhancement occurred using Gd-DTPA. Uptake of the micelles was shown, through competition experiments, to be a receptor-mediated process.[41] However, the

potential immunogenicity of antibodies and cost to generate them in a quantity may limit the use of immunomicelles clinically.[10] Small molecules or polymers are alternatives to antibodies.[42] SR-A recognizes a wide range of ligands that are polyanionic, though not all polyanionic molecules. Our results show that sulfation of dextran coated IO NPs greatly increased the negative charges on the particle surface (high negative ζ value); this allowed the particles to be recognized by SR-A and accumulate at the injured carotid artery *in vivo*. Competition studies support that the particles were taken up by a receptor-mediated uptake and not merely due to nonspecific electrostatic association.

Macrophages and macrophage scavenger receptors play a key role in the pathogenesis of atherosclerosis. Macrophages are present through all stages of atherosclerosis development, from the initiation of plaques through the formation of complex plaques containing foam cells, necrotic debris, and thrombi, and have been specifically associated with plaque stability—high densities of macrophages correlate with vulnerability to rupture.[5, 13] Our results show that SDIO can be recognized and specifically taken up by macrophages via scavenger receptor. Their specific accumulation at the injured carotid, but not the control carotid, suggests the potential to use SDIO with MRI to detect and distinguish inflamed atherosclerotic plaques.

4. Conclusion

The use of MRI is a well-established means for injury and disease diagnosis on the anatomic scale. Current advances in targeted contrast agents allow researchers to gather *in vivo* anatomic and molecular information simultaneously. IO NPs modified to target various moieties in atherosclerotic plaques have demonstrated their utility as an important tool for enhancing magnetic resonance detection of atherosclerosis at the anatomical, cellular and molecular levels.[43] However, to date, reports of targeted MRI of macrophages, a key component in the formation and development of vulnerable plaques, are relatively rare. In this paper, we sulfated dextran coated IO NPs and therefore targeted the nanoparticles to scavenger receptors on macrophages. SDIO has a high r_2 value of 95.84 $mM^{-1}s^{-1}$ and an r_2/r_1 ratio of 5.3 (37 °C, 1.4 T), therefore acts as an efficient T_2-weighted MRI contrast agent. We demonstrate that SDIO nanoparticles are specifically and avidly taken up by macrophages *via* a receptor-mediated process that labels macrophages much more efficiently than nonsulfated analogues, and produces distinct contrast in both *in vitro* and *in vivo* T_2^*-weighted MRI images. High macrophage density has been associated with atherosclerotic plaques vulnerable to rupture. Thus, the specific targeting of macrophages with the MR nanoparticle imaging agent SDIO demonstrates the potential for SDIO to facilitate detection and diagnosis plaque stability with *in vivo* MRI.

Supplementary Material

Refer to Web version on PubMed Central for supplementary material.

Acknowledgments

The authors wish to acknowledge the National Institute of Health (EB008576-01, and EB000993), the Beckman Institute at Caltech, the Center for Molecular and Genomic Imaging at UC Davis (U24 CA 110804), and the NMR award of the University of California, Davis for support of this work. We thank Dr. Xuchu Ma, Dr. Jai Woong Seo, and Bita Alaghebandan for help in IR spectroscopy, zeta potential, and animal handling, respectively.

References

1. Fuster V, Lois F, Franco M. Early identification of atherosclerotic disease by noninvasive imaging. Nat Rev Cardiol. 2010; 7:327–333. [PubMed: 20440291]

2. Wickline SA, Neubauer AM, Winter PM, Caruthers SD, Lanza GM. Molecular imaging and therapy of atherosclerosis with targeted nanoparticles. J Magn Reson Imaging. 2007; 25:667–680. [PubMed: 17347992]
3. Cyrus T, Lanza GM, Wickline SA. Molecular imaging by cardiovascular MR. J Cardiovasc Magn Reson. 2007; 9:827–843. [PubMed: 18066742]
4. Rudd JHF, Hyafil F, Fayad ZA. Inflammation imaging in atherosclerosis. Arterioscler Thromb Vasc Biol. 2009; 29:1009–1016. [PubMed: 19304673]
5. Shaw SY. Molecular imaging in cardiovascular disease: targets and opportunities. Nat Rev Cardiol. 2009; 6:569–579. [PubMed: 19621013]
6. Winter PM, Caruthers SD, Lanza GM, Wickline SA. Quantitative cardiovascular magnetic resonance for molecular imaging. J Cardiov Magn Reson. 2010; 12 Article Number: 62.
7. Sosnovik DE, Nahrendorf M, Weissleder R. Molecular magnetic resonance imaging in cardiovascular medicine. Circulation. 2007; 115:2076–2086. [PubMed: 17438163]
8. Terreno E, Castelli DD, Viale A, Aime S. Challenges for molecular magnetic resonance imaging. Chem Rev. 2010; 110:3019–3042. [PubMed: 20415475]
9. Geraldes C, Laurent S. Classification and basic properties of contrast agents for magnetic resonance imaging. Contrast Media Mol Imaging. 2009; 4:1–23. [PubMed: 19156706]
10. Cormode DP, Skajaa T, Fayad ZA, Mulder WJM. Nanotechnology in medical imaging probe design and applications. Arterioscler Thromb Vasc Biol. 2009; 29:992–1000. [PubMed: 19057023]
11. Qiao RR, Yang CH, Gao MY. Superparamagnetic iron oxide nanoparticles: from preparations to in vivo MRI applications. J Mater Chem. 2009; 19:6274–6293.
12. Croons V, Martinet W, De Meyer GRY. Selective removal of macrophages in atherosclerotic plaques as a pharmacological approach for plaque stabilization: benefits vs. potential complications. Curr Vasc Pharmacol. 2010; 8:495–508. [PubMed: 19485918]
13. Osborn EA, Jaffer FA. Advances in molecular imaging of atherosclerotic vascular disease. Curr Opin Cardiol. 2008; 23:620–628. [PubMed: 18830079]
14. Tang TY, Muller KH, Graves MJ, Li ZY, Walsh SR, Young V, et al. Iron oxide particles for atheroma imaging. Arterioscler Thromb Vasc Biol. 2009; 29:1001–1008. [PubMed: 19229073]
15. Sadat U, Li ZY, Graves MJ, Tang TY, Gillard JH. Noninvasive imaging of atheromatous carotid plaques. Nat Clin Pract Cardiovasc Med. 2009; 6:200–209. [PubMed: 19234500]
16. Gustafsson B, Youens S, Louie AY. Development of contrast agents targeted to macrophage scavenger receptors for MRI of vascular inflammation. Bioconjugate Chem. 2006; 17:538–547.
17. Tu CQ, Ma XC, Pantazis P, Kauzlarich SM, Louie AY. Paramagnetic, silicon quantum dots for magnetic resonance and two-photon imaging of macrophages. J Am Chem Soc. 2010; 132:2016–2023. [PubMed: 20092250]
18. Jarrett BR, Correa C, Ma KL, Louie AY. In vivo mapping of vascular inflammation using multimodal imaging. PLoS One. 2010; 5 Article Number: e13254.
19. de Winther MPJ, van Dijk KW, Havekes LM, Hofker MH. Macrophage scavenger receptor class A - A multifunctional receptor in atherosclerosis. Arterioscler Thromb Vasc Biol. 2000; 20:290–297. [PubMed: 10669623]
20. Jarrett BR, Frendo M, Vogan J, Louie AY. Size-controlled synthesis of dextran sulfate coated iron oxide nanoparticles for magnetic resonance imaging. Nanotechnology. 2007; 18 Article Number: 035603.
21. Tu CQ, Louie AY. Photochromically-controlled, reversibly-activated MRI and optical contrast agent. Chem Commun. 2007:1331–1333.
22. Kumar A, Hoover JL, Simmons CA, Lindner V, Shebuski RJ. Remodeling and neointimal formation in the carotid artery of normal and P-selectin-deficient mice. Circulation. 1997; 96:4333–4342. [PubMed: 9416901]
23. Heinze T, Liebert T, Heublein B, Hornig S. Functional polymers based on dextran. Adv Polym Sci. 2006; 205:199–291.
24. Mahner C, Lechner MD, Nordmeier E. Synthesis and characterisation of dextran and pullulan sulphate. Carbohydr Res. 2001; 331:203–208. [PubMed: 11322734]

25. Papy-Garcia D, Barbier-Chassefiere V, Rouet V, Kerros ME, Klochendler C, Tournaire MC, et al. Nondegradative sulfation of polysaccharides. synthesis and structure characterization of biologically active heparan sulfate mimetics. Macromolecules. 2005; 38:4647–4654.
26. Wondraczek H, Pfeifer A, Heinze T. Synthetic photocrosslinkable polysaccharide sulfates. Eur Polym J. 2010; 46:1688–1695.
27. Obeidat WM, Schwabe K, Muller RH, Keck CM. Preservation of nanostructured lipid carriers (NLC). Eur J Pharm Biopharm. 2010; 76:56–67. [PubMed: 20452422]
28. Greaves DR, Gordon S. The macrophage scavenger receptor at 30 years of age: current knowledge and future challenges. J Lipid Res. 2009; 50 S282-S6.
29. Babaev VR, Gleaves LA, Carter KJ, Suzuki H, Kodama T, Fazio S, et al. Reduced atherosclerotic lesions in mice deficient for total or macrophage-specific expression of scavenger receptor-A. Arterioscler Thromb Vasc Biol. 2000; 20:2593–2599. [PubMed: 11116058]
30. Gossuin Y, Gillis P, Hocq A, Vuong QL, Roch A. Magnetic resonance relaxation properties of superparamagnetic particles. Wiley Interdiscip Rev Nanomed Nanobiotechnol. 2009; 1:299–310. [PubMed: 20049798]
31. Tu C, Nagao R, Louie AY. Multimodal magnetic-resonance/optical-imaging contrast agent sensitive to NADH. Angew Chem Int Ed Engl. 2009; 48:6547–6551. [PubMed: 19630041]
32. O'Brien J, Wilson I, Orton T, Pognan F. Investigation of the Alamar Blue (resazurin) fluorescent dye for the assessment of mammalian cell cytotoxicity. Eur J Biochem. 2000; 267:5421–5426. [PubMed: 10951200]
33. Muller K, Skepper JN, Posfai M, Trivedi R, Howarth S, Corot C, et al. Effect of ultrasmall superparamagnetic iron oxide nanoparticles (Ferumoxtran-10) on human monocyie-macrophages in vitro. Biomaterials. 2007; 28:1629–1642. [PubMed: 17178155]
34. Metz S, Bonaterra G, Rudelius M, Settles M, Rummeny EJ, Daldrup-Link HE. Capacity of human monocytes to phagocytose approved iron oxide MR contrast agents in vitro. Eur Radiol. 2004; 14:1851–1858. [PubMed: 15249981]
35. Schulze E, Ferrucci JT, Poss K, Lapointe L, Bogdanova A, Weissleder R. Cellular uptake and trafficking of a prototypical magnetic iron-oxide label in-vitro. Invest Radiol. 1995; 30:604–610. [PubMed: 8557500]
36. Mailander V, Lorenz MR, Holzapfel V, Musyanovych A, Fuchs K, Wiesneth M, et al. Carboxylated superparamagnetic iron oxide particles label cells intracellularly without transfection agents. Mol Imaging Biol. 2008; 10:138–146. [PubMed: 18297365]
37. Sun C, Lee JSH, Zhang MQ. Magnetic nanoparticles in MR imaging and drug delivery. Adv Drug Deliv Rev. 2008; 60:1252–1265. [PubMed: 18558452]
38. Sosnovik DE, Caravan P. Molecular MRI of atherosclerotic plaque with targeted contrast agents. Curr Cardiovasc Imaging Rep. 2009; 2:87–94. [PubMed: 20019886]
39. Nahrendorf M, Zhang HW, Hembrador S, Panizzi P, Sosnovik DE, Aikawa E, et al. Nanoparticle PET-CT imaging of macrophages in inflammatory atherosclerosis. Circulation. 2008; 117:379–387. [PubMed: 18158358]
40. Uppal R, Caravan P. Targeted probes for cardiovascular MRI. Future Med Chem. 2010; 2:451–470. [PubMed: 20539821]
41. Amirbekian V, Lipinski MJ, Briley-Saebo KC, Amirbekian S, Aguinaldo JGS, Weinreb DB, et al. Detecting and assessing macrophages in vivo to evaluate atherosclerosis noninvasively using molecular MRI. Proc Natl Acad Sci U S A. 2007; 104:961–966. [PubMed: 17215360]
42. Choudhury RP, Fisher EA. Molecular imaging in atherosclerosis, thrombosis, and vascular inflammation. Arterioscler Thromb Vasc Biol. 2009; 29:983–991. [PubMed: 19213945]
43. Thorek DLJ, Chen A, Czupryna J, Tsourkas A. Superparamagnetic iron oxide nanoparticle probes for molecular imaging. Ann Biomed Eng. 2006; 34:23–38. [PubMed: 16496086]

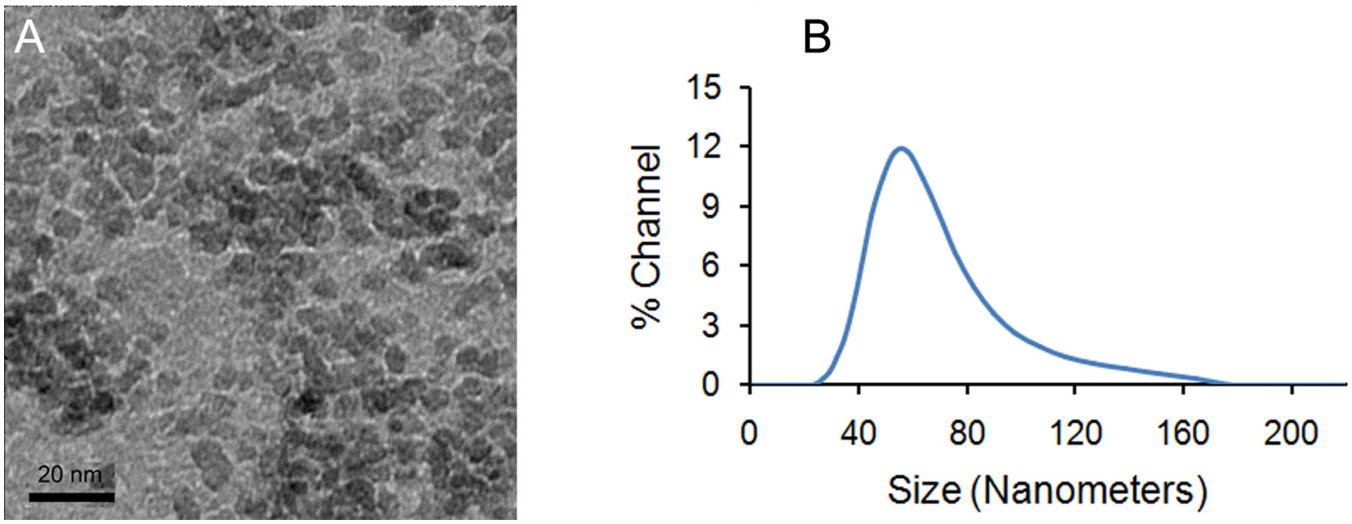

Fig. 1.
(a) TEM, and (b) DLS of dextran sulfate coated iron oxide nanoparticles (SDIO).

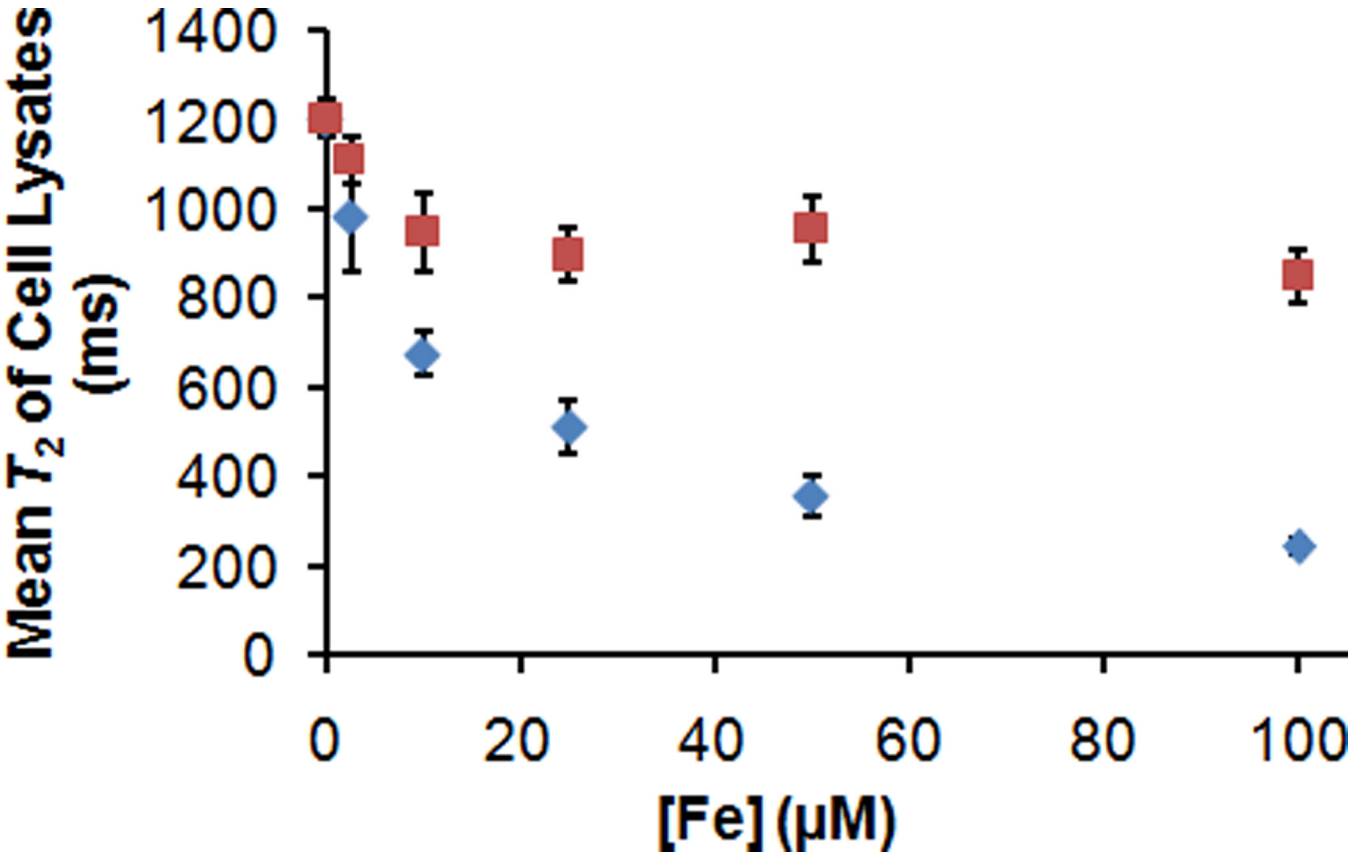

Fig. 2.
Mean T_2 values of cell lysates incubated for 2 h with SDIO (♦) or DIO (■) of different iron concentrations.

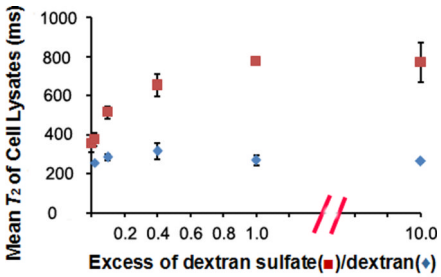

Fig. 3.

Competitive uptake of SDIO ([Fe] = 5.0×10^{-5} M) and dextran sulfate (■), or dextran (♦) by P388D1 cells.

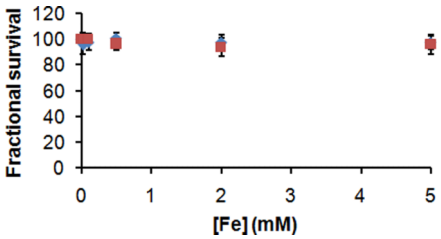

Fig. 4.
Cell viability of P388D1 after 4- (♦), or 24-h (■) incubation with different concentrations of SDIO.

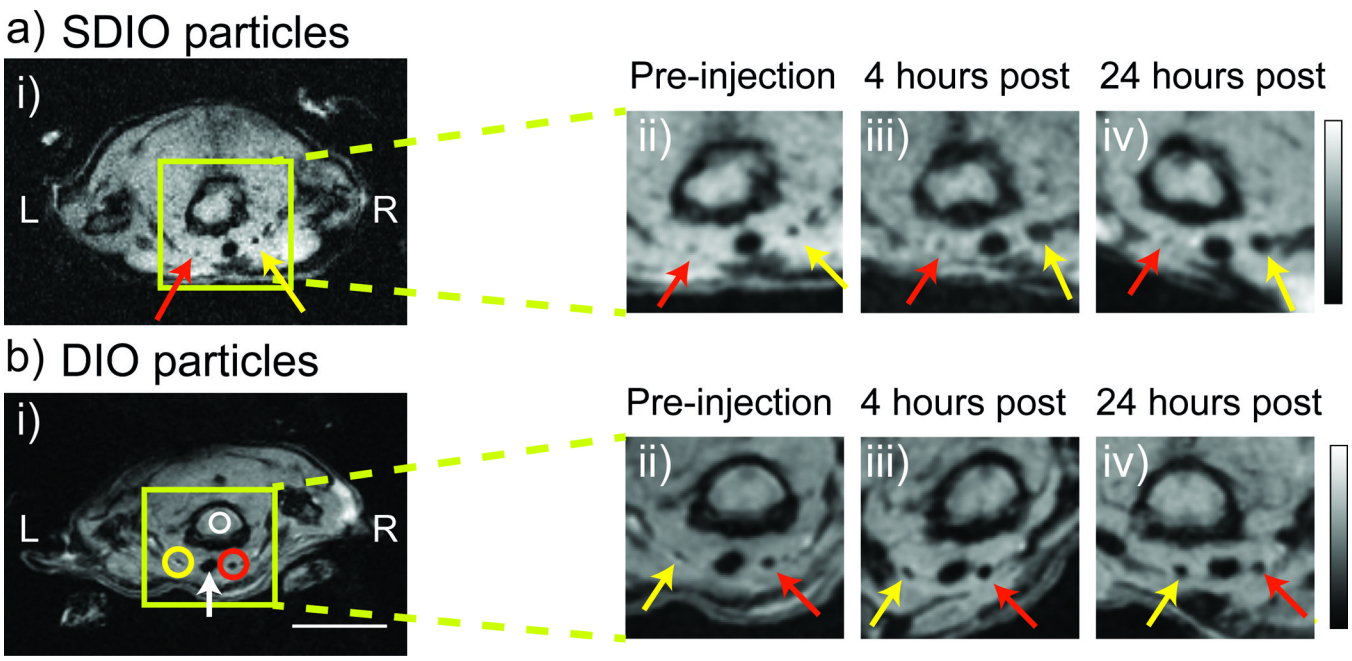

Fig. 5.

Signal change in MRI over time after SDIO (a) or DIO (b) injection. The ligated carotid artery is denoted by the yellow arrow and the control carotid artery is denoted by the red arrow. Circles indicate the ROI measures used to derive the contrast ratio (CR) metric. To facilitate comparison, the magnified images in carotid areas were first rotated in plane so all time points in the orientation. They were then zero-filled by a factor of 2 and then smoothed with a 2×2 Gaussian filter. (Scale bar = 10 mm, both scale bar and intensity bar apply to the whole animal images only. L = left, R = right, green box shows magnification area, white arrow denotes the trachea)

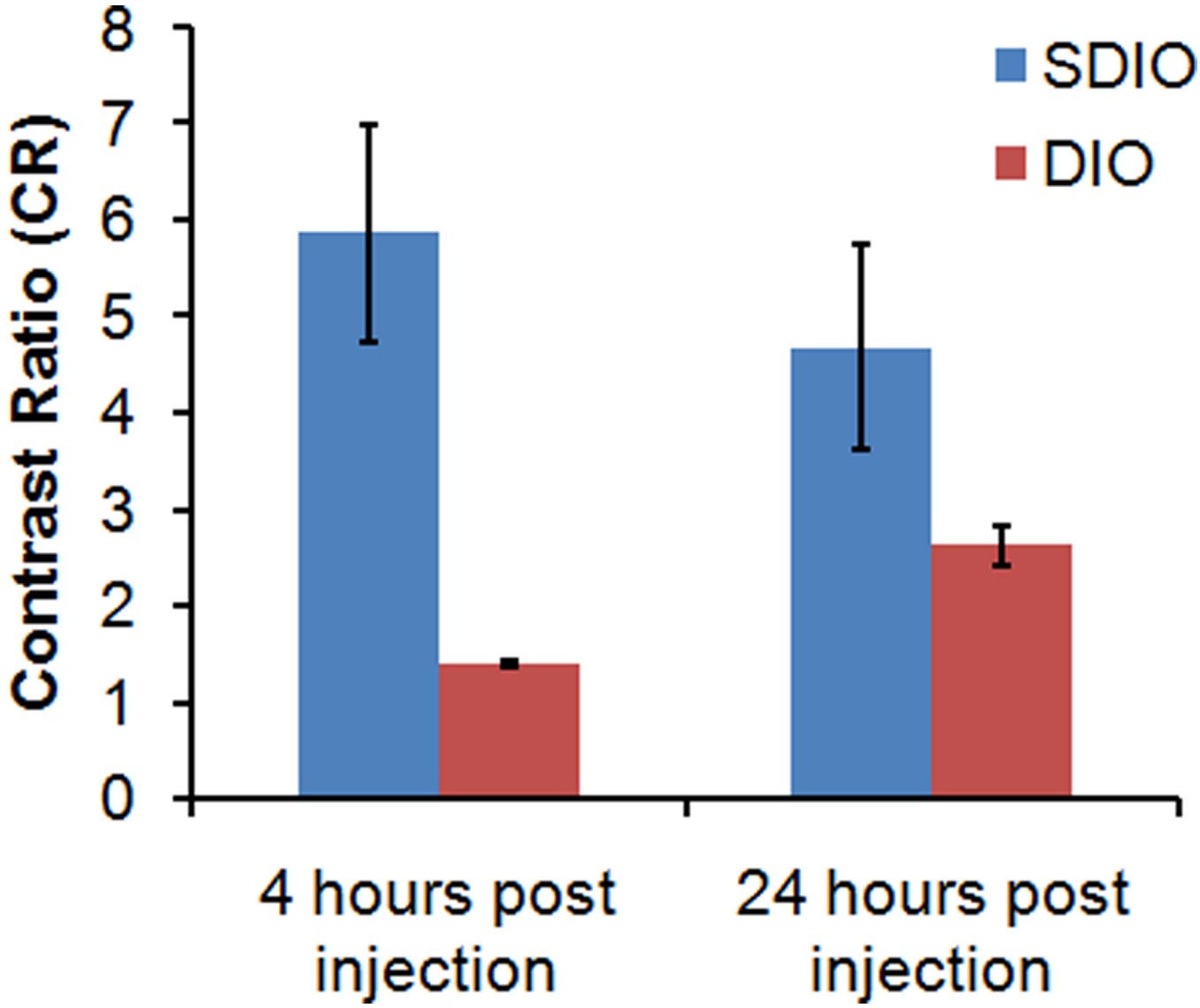

Fig. 6.
Contrast Ratio between SDIO and DIO particle accumulation *in vivo*.

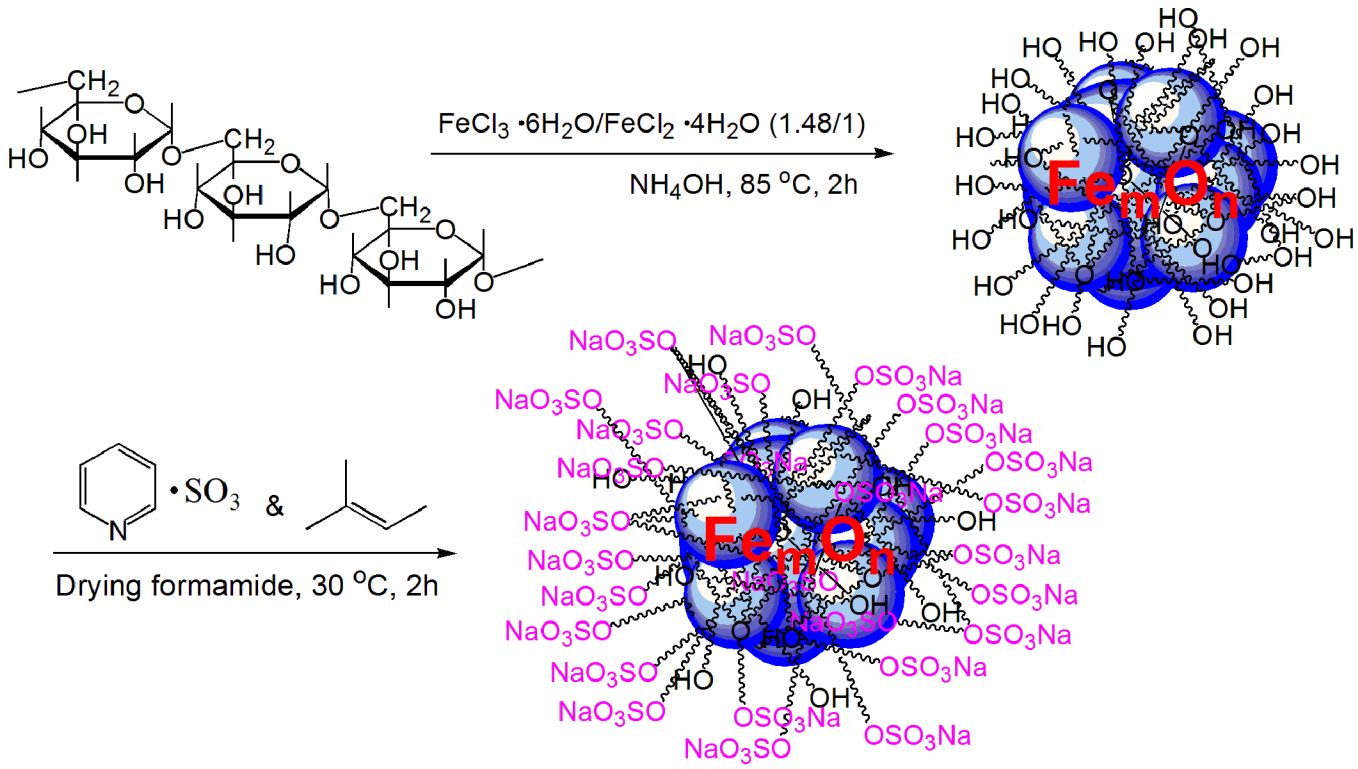

Scheme 1.
Sulfation of dextran coated iron oxide nanoparticles.

Table 1

Characteristics of dextran sulfate coated iron oxide nanoparticles (SDIO), in comparison with dextran coated iron oxide nanoparticles (DIO) and commercially available dextran coated iron oxide nanoparticles (Sinerem).

Nanoparticles	Core size (nm)	Average hydrodynamic diameter (nm)	Relaxivity ($mM^{-1}s^{-1}$) (1.4 T, 37 °C)		% iron	ζ (mV)
			r_1	r_2		
SDIO	7–8	62.4	18.1	95.8	11.34	− 40.05
DIO	7–8	42.4	15.7	89.2	17.7	− 14.90
Sinerem	N/A	< 50 nm	19.5*	87.6*	N/A	N/A

* 1.5 T, 37 °C